A&A 635, A99 (2020)
https://doi.org/10.1051/0004-6361/201936630

Astronomy & Astrophysics

Reionization optical depth determination from *Planck* HFI data with ten percent accuracy

L. Pagano[1,2,3,4], J.-M. Delouis[5,3,6], S. Mottet[3,6], J.-L. Puget[4,2,3], and L. Vibert[2,3]

[1] Dipartimento di Fisica e Scienze della Terra, Università degli Studi di Ferrara and INFN – Sezione di Ferrara, Via Saragat 1, 44122 Ferrara, Italy
e-mail: luca.pagano@unife.it, pgnlcu@unife.it
[2] Institut d'Astrophysique Spatiale, CNRS, Univ. Paris-Sud, Université Paris-Saclay, Bât. 121, 91405 Orsay Cedex, France
[3] Institut d'Astrophysique de Paris, CNRS (UMR7095), 98bis boulevard Arago, 75014 Paris, France
[4] LERMA, Sorbonne Université, Observatoire de Paris, Université PSL, École Normale Supérieure, CNRS, Paris, France
[5] Laboratoire d'Océanographie Physique et Spatiale (LOPS), Univ. Brest, CNRS, Ifremer, IRD, Brest, France
[6] Sorbonne Université, UMR7095, 98bis boulevard Arago, 75014 Paris, France

Received 3 September 2019 / Accepted 26 January 2020

ABSTRACT

We present an estimation of the reionization optical depth τ from an improved analysis of data from the High Frequency Instrument (HFI) on board the *Planck* satellite. By using an improved version of the HFI map-making code, we greatly reduce the residual large-scale contamination affecting the data, characterised in, but not fully removed from, the *Planck* 2018 legacy release. This brings the dipole distortion systematic effect, contaminating the very low multipoles, below the noise level. On large-scale polarization-only data, we measure $\tau = 0.0566^{+0.0053}_{-0.0062}$ at 68% C.L., reducing the *Planck* 2018 legacy release uncertainty by ∼40%. Within the ΛCDM model, in combination with the *Planck* large-scale temperature likelihood, and the high-ℓ temperature and polarization likelihood, we measure $\tau = 0.059 \pm 0.006$ at 68% C.L., which corresponds to a mid-point reionization redshift of $z_{\rm re} = 8.14 \pm 0.61$ at 68% C.L. This estimation of the reionization optical depth with 10% accuracy is the strongest constraint to date.

Key words. cosmic background radiation – dark ages, reionization, first stars – methods: data analysis

1. Introduction

Cosmological recombination around redshift $z = 1100$ produces a mostly neutral universe, starting the so-called dark ages. At later stages, the Universe's dark ages end with the formation of the first galaxies. The lack of Gunn-Peterson trough (Gunn & Peterson 1965; Scheuer 1965) in the spectra of distant quasars (Rauch 1998; Becker et al. 2001; Fan et al. 2006) revealed that the Universe had become almost fully reionised by redshift $z \simeq 6$ (Dayal & Ferrara 2018).

In the context of cosmological observations, cosmic microwave background (CMB) generated at the time of recombination and propagating almost freely towards us, is mostly influenced by the total amount of free electrons along the line of sight, parametrised by the Thomson scattering optical depth to reionization τ, one of the six parameters of the Λ cold dark matter (ΛCDM) model.

Reionization has two main effects on cold dark matter (CDM) power spectra. Firstly, it damps scalar perturbations by a factor $e^{-2\tau}$ as generated at recombination. This makes the amplitude $A_{\rm s}$ of the scalar perturbation highly degenerate with τ for high multipole measurements. Secondly, the rescattering of the CMB photons on free electrons at the reionization epoch generates a bump on polarization power spectra at large angular scales. The position and height of this bump depend on the mean reionization redshift ($z_{\rm re}$) and on the duration of the reionization transition. The measured quantity on the spectra at high multipoles is $A_{\rm s}e^{-2\tau}$, and thus $\delta A_{\rm s}/A_{\rm s} = 2\delta\tau$. The measurement of the large-scale polarization makes it possible to break the degeneracy with $A_{\rm s}$ and directly provides τ. A ten percent relative accuracy on τ corresponds to a 1% accuracy on $A_{\rm s}$ if τ is about 0.05. The direct measurement of τ on the reionization peak is thus critical.

Although the reionization optical depth determination has been greatly improved in the last two decades, τ is still the less constrained parameter of the ΛCDM model (Weiland et al. 2018; Planck Collaboration VI 2019). The reionization peak being visible only at very large scales ($\ell < 10$), both in EE and TE spectra, it has only been directly measured on full sky-polarised observations by space experiments. The first measurement from *Wilkinson* Microwave Anisotropy Probe (WMAP; Kogut et al. 2003) gave $\tau = 0.17 \pm 0.04$ based on the TE spectrum, while on the final 9-yr WMAP maps Hinshaw et al. (2013) reported $\tau = 0.089 \pm 0.014$ measured on TE and EE spectra. *Planck* collaboration in a re-analysis of the WMAP maps (Planck Collaboration V 2019) used the *Planck* 353 GHz map as dust tracer rather then the WMAP dust template (Page et al. 2007), based on the starlight-derived polarization directions and the Finkbeiner–Davis–Schlegel dust model (Finkbeiner et al. 1999), lowering τ by roughly 2σ to $\tau = 0.062 \pm 0.012$.

Using *Planck* only data and the Low Frequency Instrument (LFI) 70 GHz (Planck Collaboration II 2020) map as the main cosmological channel, the Planck Collaboration found compatible values of $\tau = 0.067 \pm 0.023$ in the 2015 release (Planck Collaboration XI 2016) and $\tau = 0.063 \pm 0.020$ in the 2018 legacy release (Planck Collaboration V 2019). After the *Planck* 2015 release, Lattanzi et al. (2017) reanalysed all the available datasets and combined LFI 2015 data with WMAP finding $\tau = 0.066^{+0.012}_{-0.013}$.

All those results are obtained using the same general method, so, CMB maps are cleaned of foreground contamination and then the probability is directly computed on maps assuming Gaussian signal and noise (Tegmark 1996; Page et al. 2007; Lattanzi et al. 2017). This relies on accurate estimation of the noise bias covariance matrix. An exhaustive review of all the measures before the *Planck* 2018 legacy release can be found in Weiland et al. (2018).

For the *Planck* HFI data, which is more sensitive than WMAP and LFI channels, but more vulnerable to systematic effects, a different approach was followed by the Planck Collaboration. In this case, given the difficulty of estimating reliable covariance matrices, a spectrum based likelihood was developed, acting on the cross-spectrum of 100 and 143 GHz maps. Following this approach, Planck Collaboration Int. XLVI (2016) measured $\tau = 0.055 \pm 0.009$ in an intermediate analysis of HFI data after the *Planck* 2015 release, while $\tau = 0.051 \pm 0.009$ is reported in the *Planck* 2018 legacy release (Planck Collaboration V 2019)[1]. Overall, still the major limitation is the presence of large-scale systematic effects, highly reduced with respect to *Planck* 2015 analysis but not brought below the noise level.

For a clearer global picture, we report the main τ constraints to date, in the base ΛCDM model, for different large-scale CMB datasets:

$$\begin{aligned}
&\tau = 0.089 \pm 0.013 \quad Ka,\ Q,\ \text{and},\ V \text{ with the WMAP dust model},\\
&\tau = 0.062 \pm 0.012 \quad Ka,\ Q,\ \text{and},\ V \text{ cleaned by 353 GHz},\\
&\tau = 0.063 \pm 0.020 \quad \text{LFI 70 GHz},\\
&\tau = 0.051 \pm 0.009 \quad \text{HFI } 100 \times 143 \text{ GHz}, \qquad (1)
\end{aligned}$$

where the first value reported represents the final bound of WMAP Collaboration; the second is the most recent WMAP bound when the *Planck* 353 GHz map is used for the thermal dust cleaning; the last two values represent the *Planck* 2018 legacy release bounds obtained using LFI and HFI, respectively.

In this paper, we present an advanced approach to the *Planck* HFI data in an attempt to reduce the systematic effects affecting the large-scale polarization with the purpose of improving and solidifying the constraints of τ. We upgraded the `SRoll` map-making algorithm introduced in Planck Collaboration Int. XLVI (2016, hereafter `SRoll1`) with a new cleaning of residual distortions of the large signals, we call this new algorithm `SRoll2` (Delouis et al. 2019).

The paper is organised as follows: in Sect. 2, we present the improved map-making algorithm. In Sects. 3 and 4, we present the power spectra, the main result on τ, and the consistency tests performed. Finally, in Sect. 5, we show the impact of the new τ constrain on the cosmological scenario.

2. Map-making improvements

The 2018 legacy HFI maps (Planck Collaboration III 2020) represent a great step forward in the attempt to clean systematic effects contaminating the large-scale polarization. In particular, the impact of the non-linearities of the analogue-to-digital converters (ADCs) of readout chains has been substantially reduced, introducing variation in the gain of bolometer readout chains. This correction accounts for the first-order approximation of the ADC non-linearity (ADCNL) systematic effect, but still, large signals, such as foregrounds on the Galactic plane and dipoles, are affected by the second-order ADCNL effect. This was not treated by the Planck Collaboration (see Sect. 5.13 of Planck Collaboration III 2020 for details), leaving large-scale residuals in polarization mainly due to a mismatch that, violating the stationarity of the signal in a given pixel, causes temperature to polarization dipole leakage.

For the analysis presented in this paper, we improve the `SRoll1` code in what we call `SRoll2`, in order to further reduce the polarization leakage due to strong signals. In the following, we describe the main modifications introduced in the `SRoll2` code, for more details, see Delouis et al. (2019).

(1) A new ADCNL correction is obtained by fitting the residuals with a bi-dimensional spline model per bolometer as a function of signal value and time. This solution removes the apparent gain variation of bolometers making it possible to fit only one gain for the entire mission. As demonstrated in Delouis et al. (2019), time variation is only necessary to capture the ADCNL at 143 GHz, and thus for the 100 and 353 GHz bolometers, only a mono-dimensional spline is considered. We verify that, for those channels, opening the time variation does not improve the solution substantially.
(2) We introduce an internal fit (and subsequently marginalisation over) of the polarization angle and polarization efficiency per bolometer.
(3) We update of the CO template based on the 2015 *Planck* release, used for the bandpass mismatch fit, introducing two new templates based on ^{12}CO and ^{13}CO extracted as described in Planck Collaboration III (2020) Sect. 3.1.3 and in Delouis et al. (2019) Sect. 4.1.
(4) We update of the thermal dust template using a map based on 2018 legacy release (for details, see Sect. 4.1 of Delouis et al. 2019).
(5) We update of the real part of the empirical transfer function used at 353 GHz, replacing the 3 real harmonic ranges of the spin frequency used in the *Planck* 2018 legacy release (see Planck Collaboration III 2020; Sect. 2.2.2) by a single 10 s time constant (for details, see Sect. 4.2.2 of Delouis et al. 2019).

Figure 1 shows polarization intensity maps (defined as $P \equiv \sqrt{Q^2 + U^2}$) at 100 and 143 GHz obtained simulating realistic sky signal affected by ADCNL and projected with `SRoll1` and `SRoll2` codes. From those maps, we remove the input sky. In the first row, we show maps obtained with `SRoll1` without gain variation. In the middle row, the maps are obtained using `SRoll1` opening the gain variation and fitting 128 gain steps as was done in Planck Collaboration III (2020). In the last row, the simulated timelines are projected into maps with the `SRoll2` code. The large-scale dipole leakage present in the first panel is substantially reduced by the introduction of gain variability (second panel) which still leaves $\sim 1\,\mu$K level residuals w in Planck Collaboration III (2020). This residual is further reduced by `SRoll2`, demonstrating that the ADC–NL correction makes it possible to fit a single gain for the bolometers, as expected from pre-flight analysis (Holmes et al. 2008; Pajot et al. 2010; Catalano et al. 2010).

In Fig. 2, we report the EE pseudo power spectra ($\mathcal{D}_\ell \equiv \ell(\ell+1)C_\ell/2\pi$) of the residual systematic effects (hereinafter systematics) maps shown in Fig. 1. The level of those residuals is pushed below $2 \times 10^{-2}\,\mu\text{K}^2$ both for 100 and 143 GHz by `SRoll2`, gaining an order of magnitude with respect to `SRoll1` results. Furthermore, those residuals are weakly correlated, as can be seen in Fig. 3. In the 100×143 EE cross-spectrum, the level of systematics is further reduced below $3 \times 10^{-3}\,\mu\text{K}^2$ (green line of Fig. 3). With `SRoll2`, systematics are negligible with

[1] A more conservative analysis based on pseudo-C_ℓ estimator (Hivon et al. 2002; Tristram et al. 2005) is presented in Planck Collaboration Int. XLVII (2016) which reports $\tau = 0.058 \pm 0.012$.

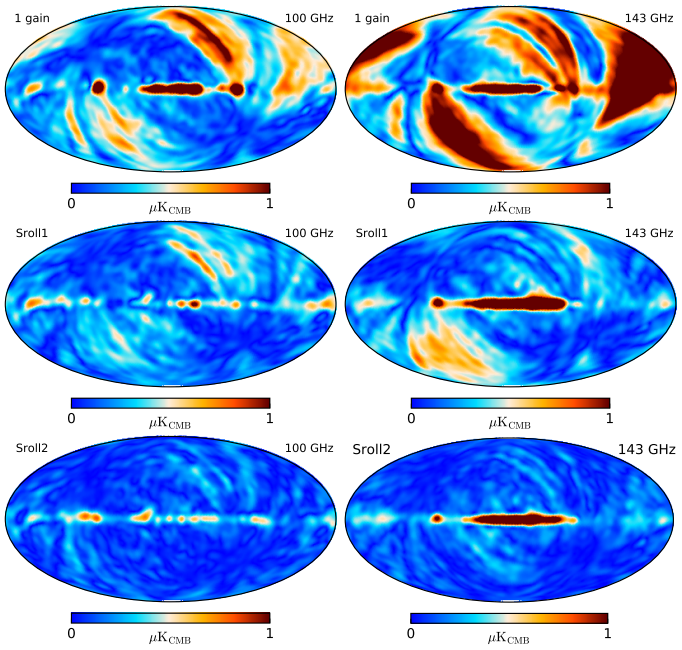

Fig. 1. Polarization intensity maps at 100 and 143 GHz obtained applying `SRoll1` and `SRoll2` to a set of simulated timelines. The input sky has been subtracted after the map projection. The simulated timelines contain dipole, sky signal, systematic effects and electronic noise only. *First row*: maps obtained running `SRoll1` with only one gain for the entire mission, *middle row*: `SRoll1` with 128 gain steps, as used in the *Planck* 2018 legacy release, and *bottom row*: `SRoll2` results.

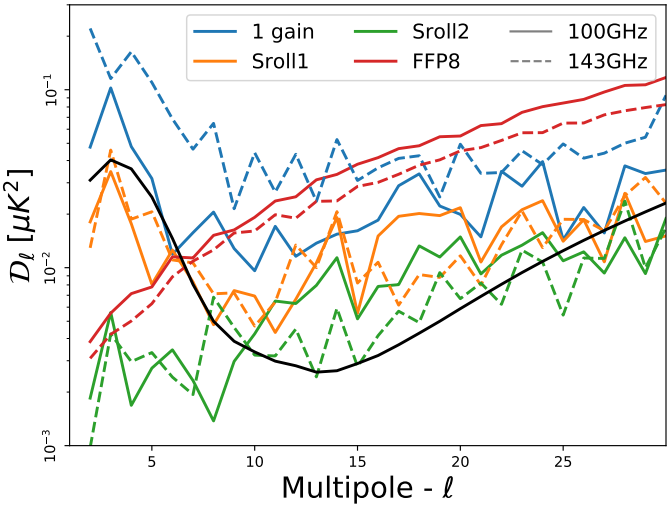

Fig. 2. EE pseudo auto-spectra evaluated for 100 GHz (solid) and 143 GHz (dashed) on the simulations shown in Fig. 1. Here we apply a symmetric Galactic cut of 20°, retaining 66% of the sky. The rise at higher multipoles is caused by the autocorrelation of the electronic noise present in the maps which is not debiased. The red lines represent the average of 100 FFP8 simulations (Planck Collaboration XII 2016) containing only white noise and $1/f$ noise. The black solid line corresponds to a EE power spectrum with $\tau = 0.055$.

respect to a typical CMB power spectrum and below the Gaussian noise level[2]. Besides, we start to be limited by the quality

[2] The noise spectrum shown in Fig. 3 should not be interpreted as noise level biasing the cross-spectrum estimate, by definition unbiased, but as noise contribution entering, together with the theoretical CMB spectrum, in the error computation.

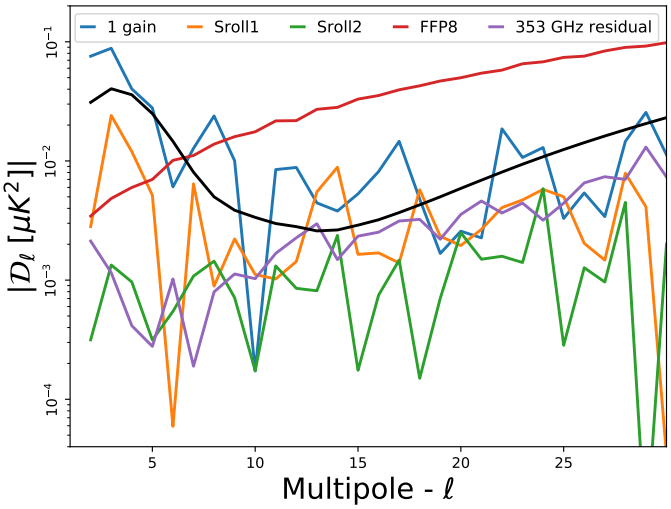

Fig. 3. As Fig. 2 but for the pseudo 100 × 143 cross-spectra. In purple, we plot the auto-spectrum of 353 GHz residual systematic effects rescaled to 100 × 143 (∼8×10^{-4} factor applied, ∼0.02 from 100 GHz and ∼0.04 from 143 GHz). The red line is the square root of the product of 100 and 143 GHz noise spectra that is proportional to the variance associated with the noise in the cross-spectrum. In the `SRoll2` maps, the large scale is dominated by signal and $1/f$ noise rather than residual systematic effects.

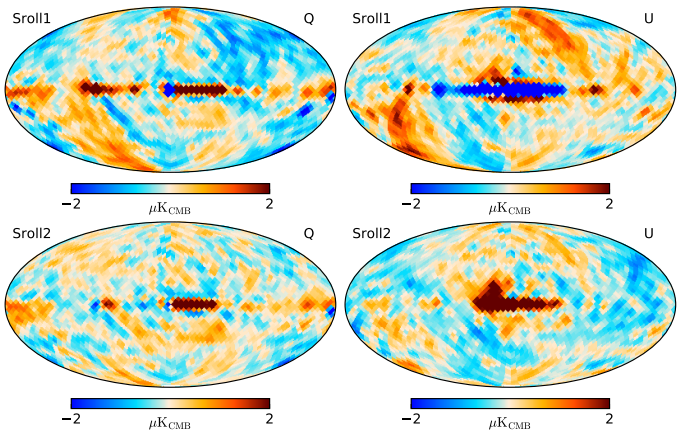

Fig. 4. Data Q and U maps at 100 GHz cleaned from synchrotron and dust emissions. *Top row*: *Planck* 2018 legacy release computation obtained with `SRoll1`, while *bottom row*: `SRoll2` computation.

of the dust template, given that the level of residual systematic effects in the 100 × 143 spectrum (green line of Fig. 3) is below, or at most equal to, the systematics still present in the 353 GHz channel used as a dust template for both 100 and 143 GHz (purple line).

Similar improvement is easily recognizable in `SRoll2` maps of data. In Figs. 4 and 5, we show 100 and 143 GHz maps after the removal of diffuse Galactic foreground contamination for both `SRoll1` and `SRoll2`. The overall level of systematics is significantly reduced everywhere in the maps by `SRoll2`. Both the large-scale spurious structures associated with dipole leakage and the Galactic disc residuals are substantially improved.

3. Power spectrum

This section describes the power spectrum computation made using `SRoll2` maps and the analysis performed on simulations.

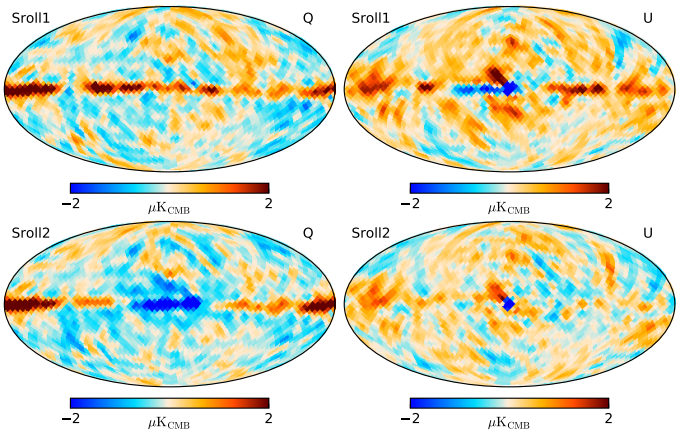

Fig. 5. Data Q and U maps at 143 GHz cleaned from synchrotron and dust emissions. *Top panel*: *Planck* 2018 legacy release computation obtained with `SRoll1`, while *bottom panel*: `SRoll2` computation.

As a general approach, we follow the procedure adopted for HFI low-ℓ analysis presented in Planck Collaboration V (2019, Sect. 2.2). In short, 100 and 143 GHz maps, built using only polarization sensitive bolometers (PSBs), undergo the following procedure:

(1) We filter them with a cosine window function (Benabed et al. 2009; Planck Collaboration Int. XLVI 2016), downgrading to `HEALPix` (Górski et al. 2005) $N_{\rm side} = 16$ resolution. In order to keep the covariances invertible, we add 20 nK of diagonal regularisation noise.
(2) We remove the Galactic foreground contamination through template fitting. We employ `SRoll2` 353 GHz map for thermal dust removal and WMAP 9-yr K and Ka bands for synchrotron at 100 and 143 GHz, respectively. The scalings found are reported in Table 1 reionization.
(3) We compute the cross-QML (Planck Collaboration V 2019; Tegmark 1996; Tegmark & de Oliveira-Costa 2001; Efstathiou 2006) power spectrum between 100 and 143 GHz cleaned maps (see Fig. 7) outside a Galactic mask (see Fig. 6). As a temperature map, we use the *Planck* 2018 `Commander` solution (Planck Collaboration IV 2020; Planck Collaboration V 2019) smoothed with a 440′ (∼7.3°) beam and regularised with 2 μK diagonal noise. As covariance matrices, we use FFP8 covariances (Planck Collaboration VIII 2016; Planck Collaboration XII 2016) for the HFI channels, and for WMAP K and Ka, the official 9-yr matrices (Bennett et al. 2013).

The same cleaning procedure is applied to a set of 500 Monte Carlo simulations containing realistic sky signal, noise, and systematic effects. The fiducial CMB map contained in those simulations is removed after the foreground cleaning leaving only maps with noise, systematic effects and foreground residuals, referred to hereinafter as `N+S+F-MC` (for noise, systematics, and foreground residuals Montecarlo).

As already stated in Planck Collaboration Int. XLVI (2016) and Planck Collaboration V (2019), FFP8 covariance matrices (Planck Collaboration XII 2016) represent a sub-optimal, but unavoidable, choice. The FFP8 covariance matrices are built following the method presented in Keskitalo et al. (2010, see in particular Sect. 3.2). They are assembled in two pieces, one describing the sub-baseline correlation part, which is untouched by the destriper map-making, and one describing the ring-to-ring correlation resulting from baseline resolution errors. Consequently, those matrices do not properly capture the variance of the systematic effects, but only the white and $1/f$ noise components, assuming an analytical model for the noise spectrum[3]. Despite that, since we rely on a cross-spectrum estimator, this choice does not impact the power spectrum estimate, but only its optimality (see e.g. Planck Collaboration Int. XLVI 2016; Planck Collaboration V 2019).

Table 1. Template scalings measured on data.

Channel [GHz]	$\alpha \times 10^2$	$\beta \times 10^2$
100	0.95 ± 0.07	1.86 ± 0.015
143	1.63 ± 0.21	0.0394 ± 0.014

Notes. The synchrotron tracers are WMAP K and Ka bands for 100 and 143 GHz, respectively. The dust tracer is the 353 GHz map.

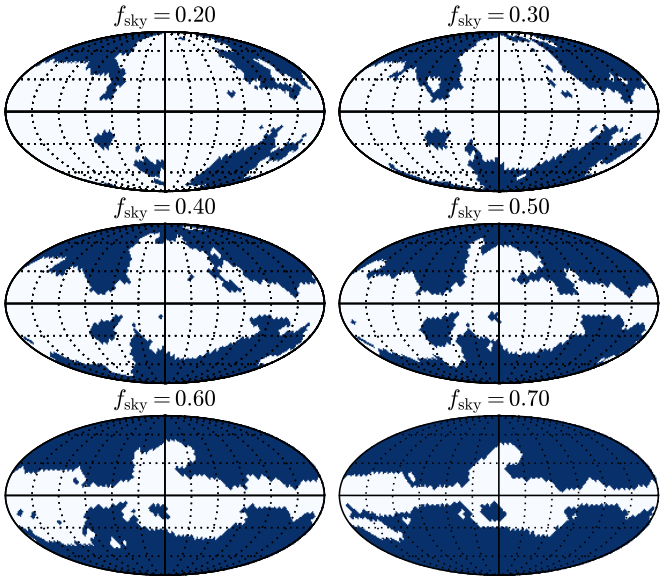

Fig. 6. Masks used for present analysis. The 70% mask is used for the foreground cleaning, the others in the cosmological analysis. All the masks used in this analysis are binary maps, without any apodisation applied.

Furthermore, for `SRoll2` maps, having the residual systematics further reduced with respect to noise (see Fig. 3), we have a more efficient estimator than the analysis performed for the *Planck* 2018 legacy release.

All masks used for foreground cleaning (see Fig. 6), power spectrum estimation, and likelihood are obtained by thresholding the sum of dust polarization intensity scaled at 143 GHz with the synchrotron polarization intensity scaled at 100 GHz, both smoothed with a Gaussian window function with full with half maximum of 7.5°. As dust and synchrotron tracers, we use *Planck* 353 GHz, scaled by $\beta = 0.039$ and WMAP K band, scaled by $\alpha = 0.0095$. The mask used for the foreground template fitting, both for data and simulations, retains 70% of the sky. The other masks are used in the cosmological analysis.

Figure 7 shows the 100 × 143 EE power spectrum of the `SRoll2` maps compared with the *Planck* 2018 power spectrum both on 50% of the sky. The error bars are obtained combining a Monte Carlo of CMB signal with $\tau = 0.055$ with `N+S+F-MC`, and computing the QML power spectrum from all the maps. The

[3] FFP8 covariance matrices can be obtained upon specific request to the *Planck* Project Scientist at ESTEC or directly to NERSC.

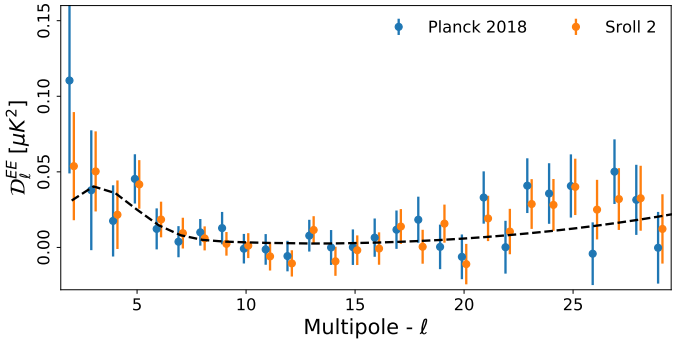

Fig. 7. Low-ℓ EE cross-spectrum 100×143 for the *Planck* 2018 legacy release (blue points) and for the `SRoll2` maps (orange). The mask used retains 50% of the sky. The error bars are Monte-Carlo-based and do include cosmic variance. The black line corresponds to a EE power spectrum with $\tau = 0.055$.

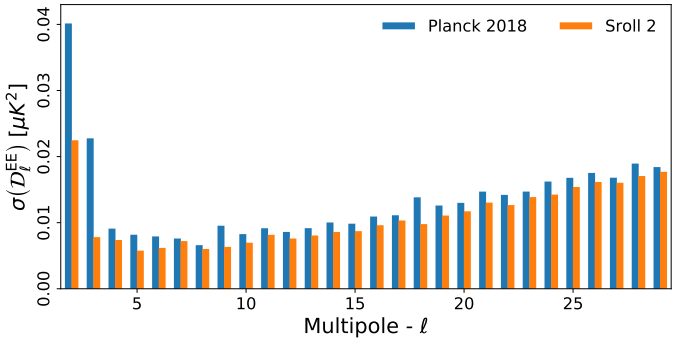

Fig. 8. Comparison between *Planck* 2018 legacy release and `SRoll2` error bars for 100×143 spectrum both on 50% of the sky. For `SRoll1`, *Planck* 2018 FFP10 Planck Collaboration III (2020) simulations have been used, for `SRoll2`, `N+S+F-MC` simulations are presented in Delouis et al. (2019). Cosmic variance is not included here.

quadrupole affecting *Planck* 2018 analysis is radically reduced by the new map-making procedure.

In Fig. 8, we compare the error bars purged from cosmic variance obtained in `SRoll2` maps with the ones of the *Planck* 2018 analysis. With the `SRoll2` maps, we manage to halve quadrupole and octupole errors with respect to the *Planck* 2018 analysis. Overall, the entire range of multipoles sensitive to reionization optical depth shows a clearly reduced level of residual systematic effects and a lower variance. Furthermore, the C_ℓs are weakly correlated, as shown in Fig. 9. In the range relevant for τ estimation $\ell = [2\dots8]$, the multipoles are substantially uncorrelated, with the scatter observed in the off-diagonal correlation perfectly compatible with the number of `N+S+F-MC` simulations. In the region where the EE signal is expected to be very small in the ΛCDM model ($\ell = [10\dots20]$), we notice the presence of a weak (up to 20%) $\ell, \ell+2$ correlation, nevertheless, this feature is not expected to affect substantially the τ estimation.

By comparing the fraction of the error due to noise and systematic effects with the cosmic variance for $\tau = 0.055$, in the range $\ell = [2\dots6]$, we notice that, for the first time, we start being dominated by the latter, as shown in Fig. 10. All the error bars are obtained using simulations and not computed analytically.

In Fig. 11, we compare the EE power spectrum obtained with different masks. The multipole $\ell = 5$ shows the largest variation throughout the various masks. We verify, using simulations, that this variation is always consistent with 2σ fluctuation.

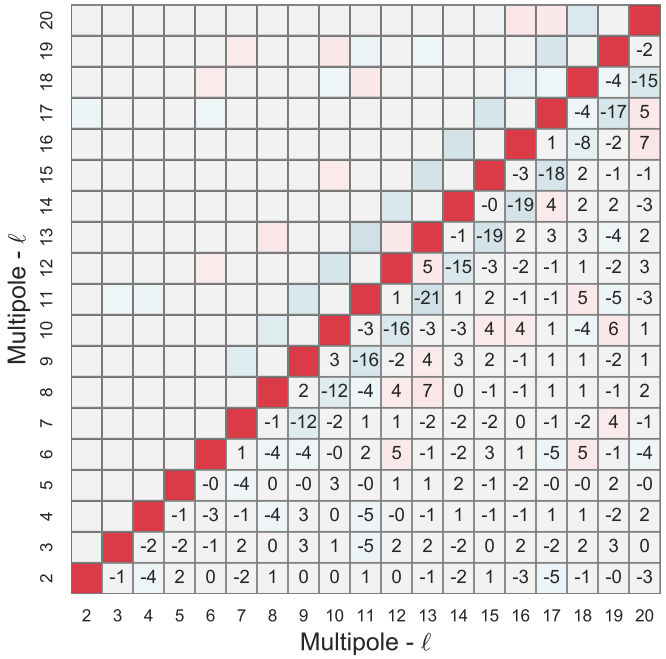

Fig. 9. Correlation matrix in [%] for EE power spectrum below $\ell = 20$ estimated from 500 signal (with $\tau = 0.055$) + `N+S+F-MC` simulations. The different multipoles are substantially uncorrelated.

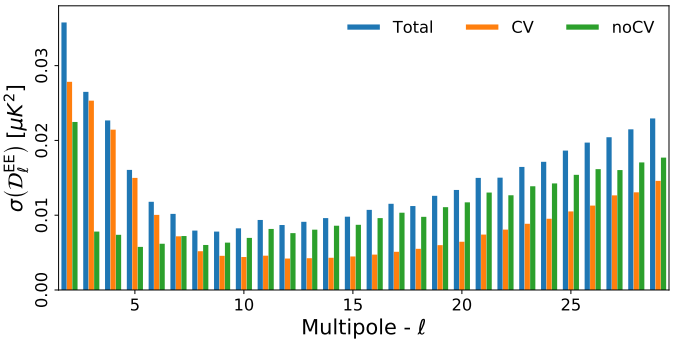

Fig. 10. Error comparison for 100×143 spectrum on 60% of the sky. We show the total error (blue bar), the amount solely due to cosmic variance (orange), and that only due to noise and systematic effects (green). The cosmic variance shown corresponds to $\tau = 0.055$.

We emphasise again that `N+S+F-MC` contains noise, systematic effects, and residuals of foreground cleaning.

As a final test, we show in Fig. 12 the BB power spectrum obtained from the cross-correlation of 100 and 143 GHz `SRoll2` maps. As a reference, we jointly plot *Planck* 2018 legacy release BB power spectrum (Planck Collaboration V 2019). Both spectra are compatible with null signal, with `SRoll2` being more constraining at a very large scale. The probability to exceed is PTE = 0.73, for *Planck* 2018, and PTE = 0.86, for `SRoll2`. The large negative quadrupole in *Planck* 2018 legacy release, related to ADCNL residuals (see Planck Collaboration III 2020; Planck Collaboration V 2019), is almost completely reabsorbed in the new analysis. As a final test, assuming the empirical distribution of the `N+S+F-MC` simulations and the power spectra measured on data computed on the 50% mask, in Table 2 we report, ℓ-by-ℓ, the percentage of simulations that have an absolute value of the difference between $\mathcal{D}_\ell$ and the barycenter of the distribution larger than the same quantity measured on data. Also in this case, the overall agreement is excellent, with no particular outliers.

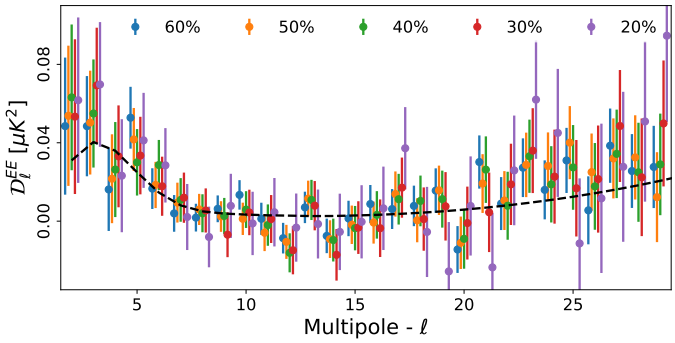

Fig. 11. EE power spectra of 100 × 143 for different sky fractions. Error bars are obtained from the distribution of 500 signal (with τ = 0.055) + N+S+F−MC simulations. The black solid line corresponds to an EE power spectrum with τ = 0.055.

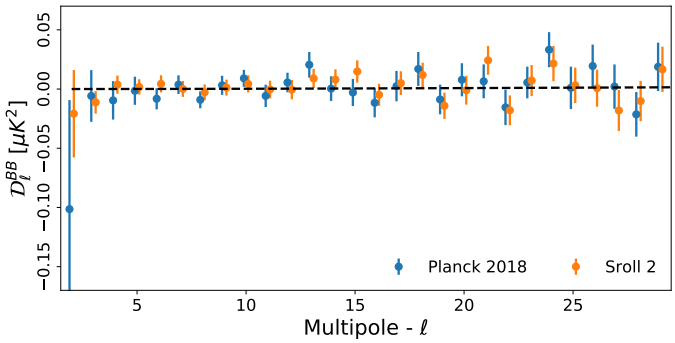

Fig. 12. Low-ℓ BB cross-spectrum 100×143 for the *Planck* 2018 legacy release (blue points) and for the SRoll2 maps (orange). The mask used retains 50% of the sky. The error bars are Monte–Carlo-based and do include cosmic variance.

Table 2. Percentage of signal plus N+S+F−MC simulations that ℓ-by-ℓ have absolute difference between $\mathcal{D}_\ell$ and the mean of the empirical distribution larger than the data.

Mulitpole	TE	EE	BB	TB	EB
2	58.1	38.0	76.5	87.5	56.2
3	72.2	20.4	6.8	42.8	90.9
4	52.8	62.5	50.1	88.5	53.9
5	28.7	93.4	52.7	23.6	27.7
6	77.7	67.1	85.4	48.2	99.8
7	93.1	91.4	35.9	68.8	72.7
8	94.2	55.4	56.0	22.7	35.5
9	99.4	83.2	12.8	43.8	93.2
10	75.0	59.1	99.3	52.1	5.6
11	16.3	62.6	46.9	37.0	52.5
12	13.9	76.8	74.1	67.2	23.7
13	24.5	32.0	95.7	91.1	39.9
14	16.9	32.4	83.5	1.8	61.8
15	52.1	12.8	98.6	2.9	7.3
16	71.5	45.4	87.0	78.9	65.7
17	38.4	75.6	89.4	86.8	59.3
18	61.4	42.3	4.1	5.9	2.4
19	32.3	13.7	11.9	84.5	14.4
20	25.6	81.2	97.5	52.3	24.0
21	43.4	8.0	70.6	31.6	51.0
22	92.5	13.4	24.7	84.6	64.0
23	34.5	68.8	91.5	22.4	35.6
24	28.8	22.3	6.1	51.9	33.6
25	17.5	93.8	40.9	15.8	57.6
26	55.4	89.1	15.1	88.1	14.5
27	55.5	21.0	84.7	3.2	26.1
28	54.6	44.4	6.4	36.2	25.2
29	76.9	57.4	86.5	88.3	91.8

4. Likelihood and τ estimation

Following the procedure presented in Planck Collaboration V (2019), we build a likelihood for τ, based on 100×143 EE power spectrum in the multipole range 2−29. In detail:

(1) we generate 101 theoretical power spectra, $C_\ell^{\rm th}(\tau, \boldsymbol{\theta})$, equally spaced in the range $\tau = [0, 0.1]$, varying accordingly $A_{\rm s}$ such that $10^9 A_{\rm s}\, e^{-2\tau} = 1.875$ as in Planck Collaboration Int. XLVI (2016). The other ΛCDM cosmological parameters ($\boldsymbol{\theta}$) are fixed to the best fit model of Planck Collaboration VI (2019);
(2) for each $C_\ell^{\rm th}(\tau, \boldsymbol{\theta})$, we build a CMB signal Monte Carlo of 500 maps;
(3) we combine N+S+F−MC with the signal Monte Carlo, and we compute the 100 × 143 EE spectrum for each realisation. We compute the power spectrum also for data, $C_\ell^{\rm data}$;
(4) by histogramming the simulations ℓ-by-ℓ and τ-by-τ, we empirically build the probability $\mathcal{P}(C_\ell|\tau;\boldsymbol{\theta})$;
(5) with a piecewise polynomial function $f_\ell(C_\ell;\tau,\boldsymbol{\theta})$, we interpolate $\ln \mathcal{P}(C_\ell|\tau;\boldsymbol{\theta})$ in order to smooth the scatter due to the limited number of simulations available;
(6) assuming negligible correlation between multipoles (see Fig. 9), we compute the probability for each τ value in our grid:

$$\mathcal{P}(\text{data}|\tau;\boldsymbol{\theta}) = \exp\left(\sum_{\ell=2}^{29} f_\ell\left(C_\ell^{\rm data};\tau,\boldsymbol{\theta}\right)\right). \quad (2)$$

With this algorithm, we can draw slices of probability for τ adopting different sky fractions and multipole ranges, in order to stress the stability of the analysis and to perform consistency tests. As a first consistency check, we test how the sky fraction used to compute the power spectrum impacts the τ constraint. We explore the same masks used in Fig. 11 and shown in Fig. 6. In Fig. 13, we show a whisker plot with best-fit values, 68% and 95% confidence levels on τ for spectra computed with different QML masks, ranging from 20 to 60% of used sky. The τ posteriors are stable, all within one σ. We verify on simulations the statistical consistency of the τ values computed on different masks, finding a consistency always better than 1.3σ throughout the various masks, having accounted for the common sky, noise, and systematics. As a baseline, we adopt the 50% mask where we measure a reionization optical depth of:

$$\tau = 0.0566^{+0.0053}_{-0.0062} \quad (68\%, \text{Sroll2 EE spectrum}), \quad (3)$$

having fixed $10^9 A_{\rm s}\, e^{-2\tau} = 1.875$. In the following part of this section, we show tests performed only on the 50% sky mask.

Figure 14 shows the effect of changing the minimum multipole used in Eq. (2). The τ posteriors are stable up to $\ell_{\rm min} = 5$, further explorations being less meaningful due to the drop of the reionization feature above those multipoles.

In Fig. 15, we test the stability of τ posterior when one multipole at a time is removed from the summation in Eq. (2). The maximum variation is observed when $\ell = 5$ is removed, causing roughly a half-σ shift in the τ posterior. This shift was consistently observed by analogous analysis performed on previous versions of the same HFI data (see e.g. Planck Collaboration Int. XLVI 2016 Fig. D.9 and Planck Collaboration V 2019 Fig. 14)

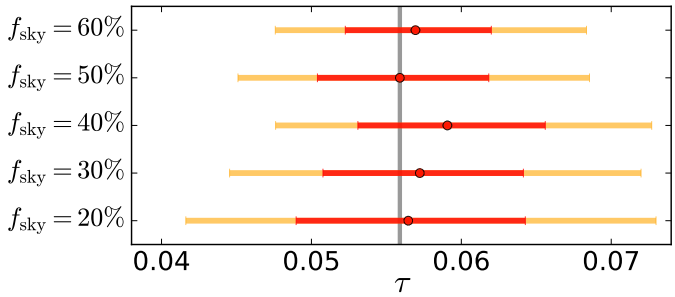

Fig. 13. Values of τ obtained varying sky fraction used for power spectrum estimation of 100×143. In this and the following plots, the round points represent best-fit values and, red and yellow bars 68% and 95% C.L., respectively.

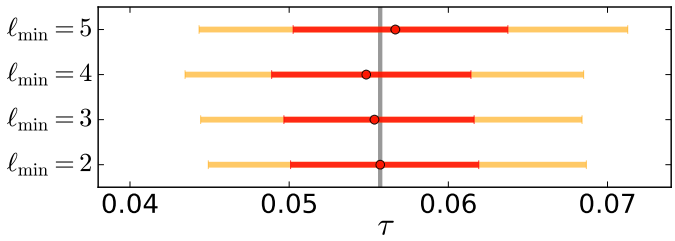

Fig. 14. Values of τ obtained changing the minimum multipole used in the likelihood code.

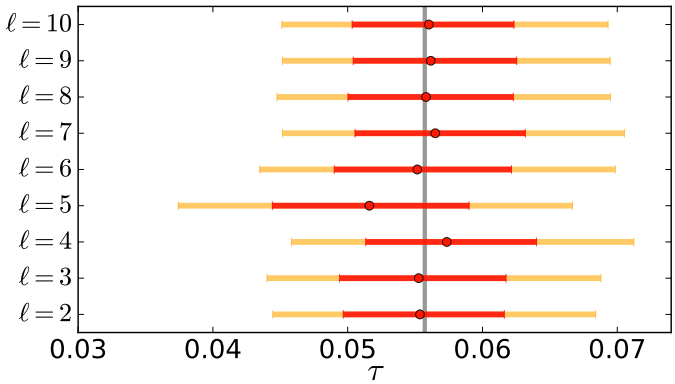

Fig. 15. Posteriors of τ obtained removing one multipole at a time.

with `SRoll2` being less discrepant despite the smaller overall error budget. Also in this case, we verify that the τ obtained removing $\ell = 5$ is consistent with a 1.2σ statistical fluctuation on the simulations when compared with the one obtained using the full range.

We also explore the stability of the τ constraint changing the synchrotron tracers used, respectively, for 100 and 143 GHz. In Fig. 16, we show τ posteriors obtained using different combinations of the available synchrotron tracers, WMAP *K* band, WMAP *Ka* band, or LFI 30 GHz (Planck Collaboration II 2020); all the posteriors are extremely consistent, demonstrating that the synchrotron subtraction does not represent a critical point, as already discussed in Planck Collaboration V (2019).

We tested the quality of the dust removal employing the 217 GHz instead of 353 GHz for the cleaning of 100 GHz. In Fig. 17, we compare the τ posterior obtained cleaning both 100 and 143 GHz using 353 GHz with the one obtained by cleaning 100 GHz with 217 GHz, and 143 GHz with 353 GHz. The consistency is remarkable, with only the latter showing slightly

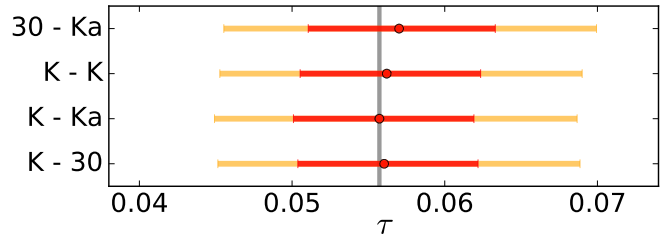

Fig. 16. Posteriors of τ obtained using different synchrotron tracers for 100 and 143 GHz. The channels reported on the left side of the figure refer to the synchrotron tracers used for 100 and 143 GHz, respectively.

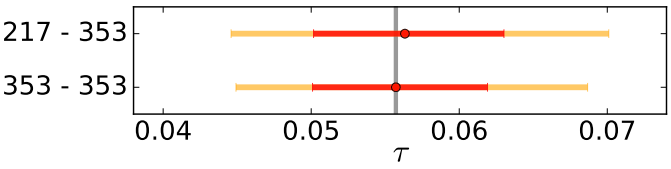

Fig. 17. Posteriors of τ obtained using different dust tracers for 100 GHz. Similarly to what is shown in Fig. 16, the channels reported in the *y*-axis label refer to the dust tracers used, respectively, for 100 and 143 GHz.

larger error bars, likely due to the smaller leverage of 217 GHz not being fully compensated by the lower noise.

Finally, we attempt a similar analysis on the TE spectrum only, measuring τ for the same 50% mask, finding:

$$\tau = 0.057^{+0.012}_{-0.013} \quad (68\%, \text{Sroll2 TE spectrum}), \tag{4}$$

which nicely confirms the EE-based result. It is worth mentioning here that the poor PTEs for the null TE spectra found in the *Planck* 2018 likelihood analysis (Planck Collaboration V 2019) are still present in this version of the data, even though with slightly less significance. We also recall that we employ the same `Commander` solution used in the *Planck* 2018 likelihood, thus based on `SRoll1` maps.

5. Impact on cosmology

Following the method presented in Planck Collaboration V (2019) and used for the *Planck* `SimAll` likelihood (i.e. lowE in *Planck* 2018 legacy release), we build a likelihood for the `SRoll2` 100×143 EE power spectrum[4]. We call this new likelihood module lowE-S2[5].

Superseding the *Planck* lowE likelihood, we combine the lowE-S2 with the high-ℓ `Plik` 2018 likelihood and with the `Commander` 2018 low-ℓ temperature likelihood in order to constrain cosmological parameters. In this section, we explore the cosmological parameter space making use of the `cosmomc`[6] package (Lewis & Bridle 2002) based on `camb`[7] Boltzmann code (Lewis et al. 2000). The global settings in terms of parametrisation and assumptions are coherent with Planck Collaboration VI (2019).

[4] For details about validation and performances of the likelihood approximation, see Gerbino et al. (2019).
[5] The likelihood module is built within the `clik` infrastructure (Planck Collaboration XV 2014; Planck Collaboration ES 2013, 2015, 2018) and it is available on `http://sroll20.ias.u-psud.fr` or on `https://web.fe.infn.it/~pagano/low_ell_datasets/sroll2`
[6] `http://cosmologist.info/cosmomc`
[7] `http://camb.info`

First of all, we combine lowE-S2 with only the Commander 2018 temperature likelihood, and we estimate the cosmological parameters only sampling $\ln(10^{10}A_s)$ and τ, keeping the other parameters fixed to *Planck* TT+lowE bestfits, measuring

$$\tau = 0.0579^{+0.0056}_{-0.0067} \quad (68\%, \texttt{Commander}\ \text{TT+lowE-S2}), \tag{5}$$

which is directly comparable with the bounds shown in Eq. (1). The amplitude of the scalar perturbations preferred by the temperature likelihood is substantially low (see e.g. Planck Collaboration V 2019 Tables 4 and 12), which is compensated by an increase of the τ value. Opening the other ΛCDM parameters and adding the TT likelihood drives the value of τ upwards

$$\tau = 0.0575^{+0.0056}_{-0.0069} \quad (68\%, \text{TT+lowE-S2}). \tag{6}$$

Similar behaviour was also observed in Planck Collaboration VI (2019) and Planck Collaboration XIII (2016) and is mainly due to the $A_s\, e^{-2\tau}$ degeneracy broken by the high-ℓ lensing in the temperature spectrum. The addition of high-ℓ polarization again drives upward A_s, and thus the optical depth, up to:

$$\tau = 0.0591^{+0.0054}_{-0.0068} \quad (68\%, \text{TT,TE,EE+lowE-S2}). \tag{7}$$

The fluctuation amplitude can be directly constrained at late times by a CMB lensing reconstruction power spectrum (Planck Collaboration VIII 2020), partially degenerated with the matter density, while the BAO measurements very efficiently constrain the geometry of the late universe (see Planck Collaboration VI 2019 for more details on those datasets). Nonetheless, the combination of *Planck* 2018 lensing likelihood and BAO measurements with the primary CMB anisotropies does not significantly improve the τ constraint:

$$\tau = 0.0599^{+0.0054}_{-0.0064} \quad (68\%, \text{TT,TE,EE+lowE-S2+Lensing+BAO}). \tag{8}$$

Assuming a tanh parametrisation of the ionisation fraction, the τ constrain can be translated into a mid-point redshift of reionization of:

$$z_{\rm re} = 8.21 \pm 0.58 \quad (68\%, \text{TT,TE,EE+lowE-S2+Lensing+BAO}), \tag{9}$$

consistent with the latest astrophysical constraint of high-redshift quasars (see e.g. Becker et al. 2001; Fan et al. 2006; Bouwens et al. 2015 for an exhaustive comparison).

The combination of low and high-ℓ likelihoods efficiently breaks the $A_s\, e^{-2\tau}$ degeneracy, giving:

$$\ln(10^{10}A_s) = 3.054 \pm 0.012 \quad (68\%, \text{TT,TE,EE+lowE-S2+Lensing+BAO}). \tag{10}$$

In the context of the ΛCDM model, this bound can be directly translated into the σ_8 parameter

$$\sigma_8 = 0.8128 \pm 0.0053 \quad (68\%, \text{TT,TE, EE+lowE-S2+Lensing+BAO}), \tag{11}$$

which measures the amplitude of the matter power spectrum on the scale of $8\,h^{-1}$ Mpc.

Bounds on the ΛCDM native parameters and some meaningful derived ones are reported in Table 3, where we compare the results obtained with the *Planck* 2018 baseline likelihood with the ones obtained replacing lowE with lowE-S2.

We also consider minimal one-parameter extensions of the ΛCDM model such as Ω_K, Σm_ν, $N_{\rm eff}$, and $Y_{\rm He}$, finding no relevant changes with respect to the *Planck* 2018 legacy release bounds (Planck Collaboration VI 2019), which reinforces the overall stability of the *Planck* 2018 results. This is likely to be connected to the mostly unchanged upper limit on τ, so, $\tau \lesssim 0.07$ at 95% C.L.

Finally, we explore the phenomenological parameter $A_{\rm L}$, which rescales the lensing potential with respect to the theoretical expectation within the ΛCDM model. Consistently throughout *Planck* releases, the CMB power spectra show a preference for $A_{\rm L} > 1$ (Planck Collaboration XVI 2014; Planck Collaboration XIII 2016; Planck Collaboration VI 2019), see Planck Collaboration Int. LI (2017) for an extensive discussion. Such values of $A_{\rm L}$ are in slight tension with the theoretical expectations and with the ones extracted from the lensing reconstruction power spectrum (Planck Collaboration VIII 2020). Combining temperature and polarization data, in the *Planck* 2018 legacy release, $A_{\rm L} = 1.180 \pm 0.065$ was measured. Replacing lowE with lowE-S2 slightly reduces the lensing amplitude down to $A_{\rm L} = 1.163 \pm 0.064$, without changing the overall conclusions of Planck Collaboration VI (2019). This is can again be explained by the increase of A_s connected with the increase of τ, which allows a slightly lower lensing amplitude.

6. Conclusions

In this paper, we present an improved constraint on the reionization optical depth τ, obtained analysing the *Planck* HFI data with an updated version of the SRoll map-making algorithm called SRoll2, specifically designed to reduce the residual large-scale polarization systematics still present in the *Planck* HFI 2018 legacy maps. Details and performances of the SRoll2 algorithm are described extensively in Delouis et al. (2019).

The level of residual systematics associated with the first multipoles, relevant for τ estimation, is brought below the noise level, and for the first time the cosmic variance becomes the main source of uncertainty in CMB large-scale polarization parameter estimation.

As explained in Planck Collaboration V (2019, see in particular Sect. 2.4), the level of T to P leakage in the *Planck* 2018 legacy release maps forced the Planck Collaboration to adopt a strategy for the large-scale polarization likelihood entirely based on simulations. Furthermore, the difficulty of building reliable covariance matrices leads to the use of a simulation-based likelihood, built on the EE cross-spectrum of 100 and 143 GHz. In the present analysis, we follow the same overall strategy, although the lower level of systematics could have allowed a semi-analytical approach (see e.g. Mangilli et al. 2015; Vanneste et al. 2018; Hamimeche & Lewis 2008; Gerbino et al. 2019), which we leave to future analysis. With this method, we measure $\tau = 0.0566^{+0.0053}_{-0.0062}$ at 68% C.L. when all the other ΛCDM parameters are kept fixed.

The main difference with respect to the *Planck* 2018 analysis (which yields $\tau = 0.051 \pm 0.009$) is based on the correction of the second-order ADCNL effect presented in Delouis et al. (2019), which drastically reduces the dipole and foreground signals distortion making it possible to recover almost completely $\ell = 2$ and $\ell = 3$ for the τ determination, suppressed in a previous analysis by a large variance (see e.g. Planck Collaboration Int. XLVI 2016; Planck Collaboration V 2019; Planck Collaboration Int. XLVII 2016). As a consequence of this in the SRoll2 EE 100 × 143 spectrum, the variance associated with systematics becomes smaller than the noise and

Table 3. Parameter constraints for the base ΛCDM cosmology (as defined in Planck Collaboration XVI 2014), illustrating the impact of replacing the lowE likelihood with the lowE-S2 likelihood presented in the paper.

Parameter	TT+lowE 68% Limits	TT+lowE-S2 68% Limits	TTTEEE+lowE 68% Limits	TTTEEE+lowE-S2 68% Limits
$\Omega_b h^2$	0.02212 ± 0.00022	0.02214 ± 0.00021	0.02236 ± 0.00015	0.02237 ± 0.00015
$\Omega_c h^2$	0.1206 ± 0.0021	0.1205 ± 0.0021	0.1202 ± 0.0014	0.1201 ± 0.0013
$100\theta_{MC}$	1.04077 ± 0.00047	1.04080 ± 0.00047	1.04090 ± 0.00031	1.04090 ± 0.00031
τ	0.0522 ± 0.0080	$0.0574^{+0.0056}_{-0.0069}$	$0.0544^{+0.0070}_{-0.0081}$	$0.0591^{+0.0054}_{-0.0068}$
$\ln(10^{10} A_s)$	3.040 ± 0.016	3.051 ± 0.013	3.045 ± 0.016	3.054 ± 0.013
n_s	0.9626 ± 0.0057	0.9631 ± 0.0056	0.9649 ± 0.0044	0.9651 ± 0.0043
H_0	66.88 ± 0.92	66.95 ± 0.90	67.27 ± 0.60	67.32 ± 0.60
Ω_m	0.321 ± 0.013	0.320 ± 0.013	0.3166 ± 0.0084	0.3158 ± 0.0082
Ω_Λ	0.679 ± 0.013	0.680 ± 0.013	0.6834 ± 0.0084	0.6842 ± 0.0082
σ_8	0.8118 ± 0.0089	0.8155 ± 0.0083	0.8120 ± 0.0073	0.8154 ± 0.0067
z_{re}	7.50 ± 0.82	8.04 ± 0.60	7.68 ± 0.79	8.14 ± 0.60
$10^9 A_s$	2.092 ± 0.034	2.113 ± 0.028	$2.101^{+0.031}_{-0.034}$	2.120 ± 0.028
$10^9 A_s e^{-2\tau}$	1.884 ± 0.014	1.884 ± 0.014	1.884 ± 0.012	1.884 ± 0.012
Age/Gyr	13.830 ± 0.037	13.827 ± 0.036	13.800 ± 0.024	13.798 ± 0.024

Notes. We also show the change when including the high-ℓ polarization.

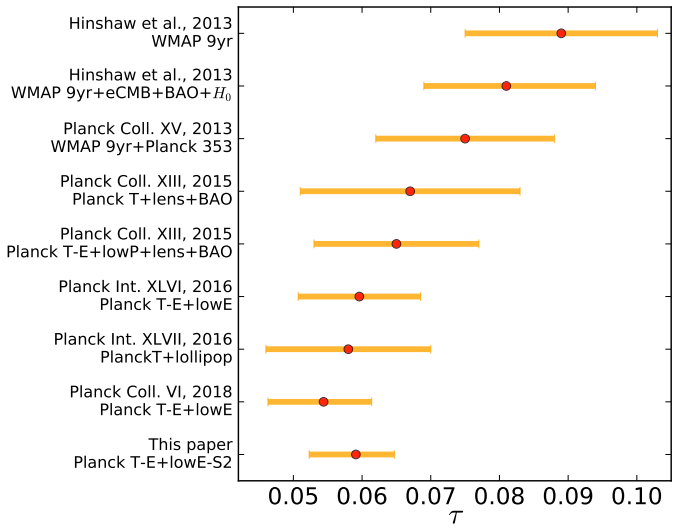

Fig. 18. History of τ determination from WMAP to *Planck*. With Planck T tag we refer to *Planck* low-ℓ and high-ℓ temperature likelihood, with Planck T-E, we refer to low-ℓ and high-ℓ temperature likelihood combined with high-ℓ TE and EE likelihood. WMAP 9-yr + Planck 353 refers to the WMAP 9-yr low-ℓ and high-ℓ likelihoods with the large-scale polarization data cleaned by *Planck* 353 GHz.

cosmic variance, making the accuracy of the ADCNL simulation produced less critical. Those aspects, together with an improved version of the foreground model, cause a ∼1-σ upward shift in the τ posterior.

In a more complete parameter exploration, combining the SRoll2 likelihood with the temperature and high-ℓ polarization likelihood, we measure $\tau = 0.059 \pm 0.006$ at 68% C.L., which represents the strongest constrain on the reionization optical depth to date. The most recent optical depth measurement from CMB data in the context of the ΛCDM model are reported in Fig. 18.

Assuming instantaneous reionization, this corresponds to $z_{re} = 8.14 \pm 0.61$ at 68% C.L. The tight bound on τ efficiently breaks the $A_s\, e^{-2\tau}$ degeneracy, reducing the constraint on the fluctuation amplitude down to $\sigma_8 = 0.8128 \pm 0.0053$ at 68% C.L.

The improvement with respect to the *Planck* 2018 legacy release in the large-scale polarization data leads to an expected reduction of the τ uncertainty, but it is matched with a slight shift upwards of the central value. This combination leads to a substantial unchanged τ upper limit, leading to a mostly unchanged constraint on all the minimal ΛCDM extensions explored. Further investigations are left to future publications. The SRoll2 data maps, simulations and, likelihood code are publicly available[8].

Acknowledgements. We acknowledge the use of CAMB, HEALPix and Healpy software packages. This work is part of the Bware project, partially supported by CNES. It was granted access to the HPC resources of CINES (http://www.cines.fr) under the allocation 2017-A0030410267 made by GENCI (http://www.genci.fr). This research used resources of the National Energy Research Scientific Computing Center (NERSC), a U.S. Department of Energy Office of Science User Facility operated under Contract No. DE-AC02-05CH11231. LP is grateful to G. Fabbian, M. Lattanzi and M. Migliaccio for many helpful discussions during the preparation of this work. LP acknowledges the support of the National Centre for Space Studies (CNES) postdoctoral program and Italian Space Agency (ASI) grant 2016-24-H.0 (COSMOS).

References

Becker, R. H., Fan, X., White, R. L., et al. 2001, ApJ, 122, 2850
Benabed, K., Cardoso, J. F., Prunet, S., & Hivon, E. 2009, MNRAS, 400, 219
Bennett, C. L., Larson, D., Weiland, J. L., et al. 2013, ApJ, 208, 20
Bouwens, R. J., Illingworth, G. D., Oesch, P. A., et al. 2015, ApJ, 811, 140
Catalano, A., Coulais, A., & Lamarre, J.-M. 2010, Appl. Opt., 49, 5938
Dayal, P., & Ferrara, A. 2018, Phys. Rep., 780, 1
Delouis, J. M., Pagano, L., Mottet, S., Puget, J. L., & Vibert, L. 2019, A&A, 629, A38
Efstathiou, G. 2006, MNRAS, 370, 343
Fan, X.-H., Strauss, M. A., Becker, R. H., et al. 2006, ApJ, 132, 117
Finkbeiner, D. P., Davis, M., & Schlegel, D. J. 1999, ApJ, 524, 867
Gerbino, M., Lattanzi, M., Migliaccio, M., et al. 2019, ArXiv e-prints [arXiv:1909.09375]
Górski, K. M., Hivon, E., Banday, A. J., et al. 2005, ApJ, 622, 759
Gunn, J. E., & Peterson, B. A. 1965, ApJ, 142, 1633
Hamimeche, S., & Lewis, A. 2008, Phys. Rev. D, 77, 103013
Hinshaw, G., Larson, D., Komatsu, E., et al. 2013, ApJS, 208, 19
Hivon, E., Gorski, K. M., Netterfield, C. B., et al. 2002, ApJ, 567, 2

[8] http://sroll20.ias.u-psud.fr

Holmes, W. A., Bock, J. J., Crill, B. P., et al. 2008, Appl. Opt., 47, 5996
Keskitalo, R., Ashdown, M. A. J., Cabella, P., et al. 2010, A&A, 522, A94
Kogut, A., Spergel, D. N., Barnes, C., et al. 2003, ApJS, 148, 161
Lattanzi, M., Burigana, C., Gerbino, M., et al. 2017, JCAP, 1702, 041
Lewis, A., & Bridle, S. 2002, Phys. Rev. D, 66, 103511
Lewis, A., Challinor, A., & Lasenby, A. 2000, ApJ, 538, 473
Mangilli, A., Plaszczynski, S., & Tristram, M. 2015, MNRAS, 453, 3174
Page, L., Hinshaw, G., Komatsu, E., et al. 2007, ApJS, 170, 335
Pajot, F., Ade, P. A. R., Beney, J., et al. 2010, A&A, 520, A10
Planck Collaboration ES. 2013, https://www.cosmos.esa.int/web/planck/pla (ESA)
Planck Collaboration ES. 2015, https://www.cosmos.esa.int/web/planck/pla (ESA)
Planck Collaboration ES. 2018, https://www.cosmos.esa.int/web/planck/pla (ESA)
Planck Collaboration XV. 2014, A&A, 571, A15
Planck Collaboration XVI. 2014, A&A, 571, A16
Planck Collaboration VIII. 2016, A&A, 594, A8
Planck Collaboration XI. 2016, A&A, 594, A11
Planck Collaboration XII. 2016, A&A, 594, A12
Planck Collaboration XIII. 2016, A&A, 594, A13
Planck Collaboration V. 2019, A&A, submitted [arXiv:1907.12875]
Planck Collaboration VI. 2019, A&A, submitted [arXiv:1807.06209]
Planck Collaboration II. 2020, A&A, in press, https://doi.org/10.1051/0004-6361/201833293
Planck Collaboration III. 2020, A&A, in press, https://doi.org/10.1051/0004-6361/201832909
Planck Collaboration IV. 2020, A&A, in press, https://doi.org/10.1051/0004-6361/201833881
Planck Collaboration VIII. 2020, A&A, in press, https://doi.org/10.1051/0004-6361/201833886
Planck Collaboration Int. XLVI. 2016, A&A, 596, A107
Planck Collaboration Int. XLVII. 2016, A&A, 596, A108
Planck Collaboration Int. LI. 2017, A&A, 607, A95
Rauch, M. 1998, ARA&A, 36, 267
Scheuer, P. A. G. 1965, Nature, 207, 963
Tegmark, M. 1996, MNRAS, 280, 299
Tegmark, M., & de Oliveira-Costa, A. 2001, Phys. Rev. D, 64, 063001
Tristram, M., Macias-Perez, J. F., Renault, C., & Santos, D. 2005, MNRAS, 358, 833
Vanneste, S., Henrot-Versillé, S., Louis, T., & Tristram, M. 2018, Phys. Rev. D, 98, 103526
Weiland, J. L., Osumi, K., Addison, G. E., et al. 2018, ApJ, 863, 161